PROCEEDINGS OF SPIE

SPIEDigitalLibrary.org/conference-proceedings-of-spie

Ultrasound to video registration using a bi-plane transrectal probe with photoacoustic markers

Cheng, Alexis, Kang, Hyun Jae, Zhang, Haichong, Taylor, Russell, Boctor, Emad

Alexis Cheng, Hyun Jae Kang, Haichong K. Zhang, Russell H. Taylor, Emad M. Boctor, "Ultrasound to video registration using a bi-plane transrectal probe with photoacoustic markers," Proc. SPIE 9786, Medical Imaging 2016: Image-Guided Procedures, Robotic Interventions, and Modeling, 97860J (24 March 2016); doi: 10.1117/12.2216644

SPIE.

Event: SPIE Medical Imaging, 2016, San Diego, California, United States

Ultrasound to video registration using a bi-plane transrectal probe with photoacoustic markers

Alexis Cheng[a], Hyun Jae Kang[a], Haichong K. Zhang[a], Jin U. Kang[b], Russell H. Taylor[a] , Emad M. Boctor[a,b,c]

[a]Dept. of Computer Science, Johns Hopkins University, Baltimore, MD, USA
[b]Dept. of Electrical and Computer Engineering, Johns Hopkins University, Baltimore, MD, USA
[c]Dept. of Radiology, Johns Hopkins University, Baltimore, MD, USA

Extended Abstract

Modern surgical scenarios typically provide surgeons with additional information through fusion of video and other imaging modalities. To provide this information, the tools and devices used in surgery must be registered together with interventional guidance equipment and surgical navigation systems. In this work, we focus explicitly on registering ultrasound with a stereo camera system using photoacoustic markers. Previous work has shown that photoacoustic markers can be used in this registration task to achieve target registration errors lower than the current available systems. Photoacoustic markers are defined as a set of non-collinear laser spots projected onto some surface. They can be simultaneously visualized by a stereo camera system and an ultrasound transducer because of the photoacoustic effect.

In more recent work, the three-dimensional ultrasound volume was replaced by images from a single ultrasound image pose from a convex array transducer. The feasibility of this approach was demonstrated, but the accuracy was lacking due to the physical limitations of the convex array transducer. In this work, we propose the use of a bi-plane transrectal ultrasound transducer. The main advantage of using this type of transducer is that the ultrasound elements are no longer restricted to a single plane. While this development would be limited to prostate applications, liver and kidney applications are also feasible if a suitable transducer is built. This work is demonstrated in two experiments, one without photoacoustic sources and one with. The resulting target registration error for these experiments were 1.07mm±0.35mm and 1.27mm±0.47mm respectively, both of which are better than current available navigation systems.

Keywords: photoacoustic imaging, ultrasound imaging, image-guided surgery, tracking

1. Introduction

Image-guided surgery systems are frequently used during surgery to provide surgeons with informational support [1]. Ultrasound is our imaging modality of choice because it is real-time and low-cost. For these systems to show their full capabilities and enable more advanced applications such as volume building or automated actuation, tools and devices must be registered together. An integral component to register these devices together is some type of interventional guidance or surgical navigation system.

Surgical navigation systems for ultrasound will typically consist of a tracking component and an ultrasound calibration component. These two components are each represented by a rigid-body transformation, and represent the ultrasound image's pose in the external tracker's coordinate system when combined. The two main types of surgical navigation systems are electromagnetic-based (EM) and optical-based [2-4]. Unlike optical-based systems, EM-based systems do not require line of sight between its tracking base and the attached sensor, leading them to be more commonly used. However, they suffer from distortion in the presence of ferromagnetic materials, whereas optical tracking does not place such restrictions on the surgical environment. Furthermore, optical tracking can provide sub-millimeter accuracy and is generally more accurate than electromagnetic tracking [5, 6].

Medical Imaging 2016: Image-Guided Procedures, Robotic Interventions, and Modeling,
edited by Robert J. Webster III, Ziv R. Yaniv, Proc. of SPIE Vol. 9786, 97860J
 · doi: 10.1117/12.2216644

Ultrasound calibration is a necessary process if one wants to use ultrasound imaging in image-guided surgery systems. This procedure recovers the unknown transformation between a sensor attached to the ultrasound transducer and the ultrasound image. Researchers have developed many different methods and phantoms for calibration [7, 8]. The interaction between these tracking solutions and ultrasound calibration is subject to error buildup from the chain of necessary frame transformations. Overall reported registration errors are about 1.7 to 3mm for artificial phantoms and 3 to 5mm for tissue [3, 4, 9, 10].

In previous work [11-14], we demonstrated a photoacoustic surgical navigation system that made improvements on some of the disadvantages of optical-based systems. This method used photoacoustic markers that are visible to both stereo camera and ultrasound, when generated on an air-tissue interface, as fiducials to register video and three-dimensional ultrasound. Previous work [15, 16] showed that a pulsed laser source can generate a photoacoustic effect in tissue. It has also been shown that a conventional ultrasound transducer is capable of receiving the signal from the photoacoustic effect [17, 18].

First of all, the line of sight requirement was relaxed. Only the photoacoustic markers projected onto the surface of the target organ needed to be within the line of sight. This is likely to occur as the target organ should almost always be in the field of view. Secondly and more importantly, ultrasound calibration is no longer necessary, increasing the registration accuracy by eliminating the need for chaining multiple frame transformations. One of the downsides of this approach was the use of a three-dimensional ultrasound transducer. The need for an ultrasound volume increases the length of required time and may place certain assumptions such as a static environment.

In more recent work [19], we demonstrated the feasibility of using a convex array transducer in place of a three-dimensional transducer. While this change improved the practicality of the system by reducing the length of time and the static environment assumption, the accuracy also decreased because of the limitations in the physical arrangement of the convex array transducer elements. In a convex array, the elements lie on a circular arc. The constraints of this geometry is lacking because the elements lie on a two-dimensional shape.

In this work, we show how a bi-plane transrectal transducer, with its elements lying in a three-dimensional configuration, can improve the accuracy, while maintaining the advantage of not using a three-dimensional transducer. We detail the key idea that enables our method and demonstrate experimental results in two scenarios with different active point sources.

2. Methods

2.1 Video to Ultrasound Registration with Photoacoustic Markers

As can be seen in figure 1, the workflow for this method remains very similar to previous work [12-14, 19], so we will briefly summarize it here. For each photoacoustic marker projection, a pair of stereo camera images are taken. Simultaneously, the channel data from the transducer, in this case a transrectal bi-plane transducer, is also acquired. The stereo camera pair is used to recover the position of the photoacoustic marker in the stereo camera system's coordinate system. The channel data is used to recover the position of the photoacoustic marker in the ultrasound transducer's coordinate system. The process of recovering this position is different than in previous work and will be described in the following section. After at least three photoacoustic markers, a registration can be found between the two point sets using any standard point set registration algorithms such as coherent point drift [20]. This registration is equivalent to tracking the ultrasound transducer in the stereo camera system's coordinate system.

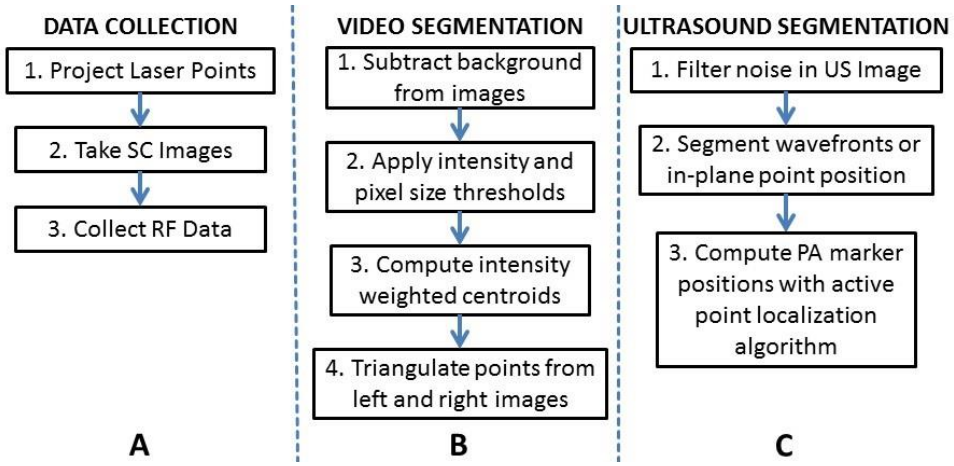

Figure 1. Experimental and Software Workflow

2.2 Active Point Localization with a Transrectal Transducer

Before we begin describing the method for localizing the active acoustic point source with respect to the transrectal transducer, we must describe the transducer itself. Bi-plane transrectal transducers typically have two imaging planes, one parallel and one perpendicular to its insertion axis. The parallel imaging plane is generally from a linear array and the perpendicular imaging plane is generally from a convex array. Figure 2 is an example of such a transducer, where the dotted lines correspond to the imaging planes. In general, these two imaging planes are perpendicular to each other

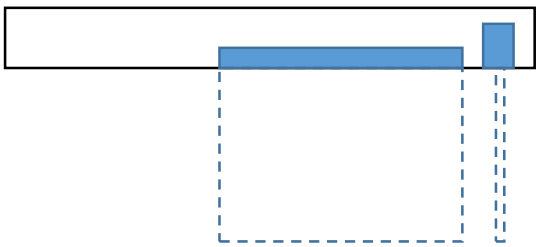
Figure 2. Ultrasound imaging planes with respect to bi-plane transrectal transducer

The key idea that enables our approach is the use of an active acoustic point source. This simply means an acoustic source where we have full control over its transmission and timing. When using an active point, the receiver will be able to capture data even if the point is outside of the probe imaging plane. Figure 3 shows an example of what the prebeamformed data of an active acoustic point source might look like in a bi-plane transrectal transducer. As highlighted by the line, it can be clearly seen that there is a delineation between the data acquired from the convex array versus the linear array.

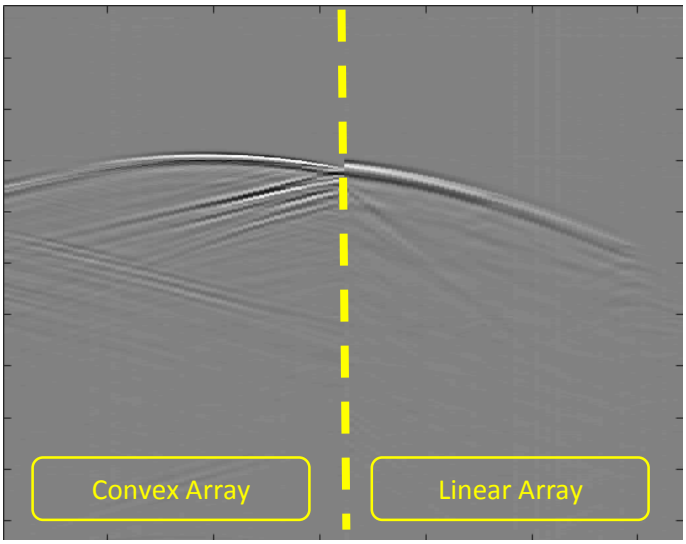

Figure 3. Sample pre-beamformed channel data from a bi-plane transrectal transducer

For example, in the scenario shown in figure 4 where the point represents an active acoustic point source, both of the transducers will receive the signal from the active acoustic point source. This property significantly increases the field of view of an ultrasound transducer. Naturally, there are still some constraints related to the transducer's receiving specifications. For example, it is unreasonable to expect the signal to be received if the active acoustic point source is tens of centimeters away normal to the imaging plane as there is some angular sensitivity to the transducer's receiving elements. The actual constraint will depend on this angular sensitivity as well as the strength of the transmitted acoustic signal.

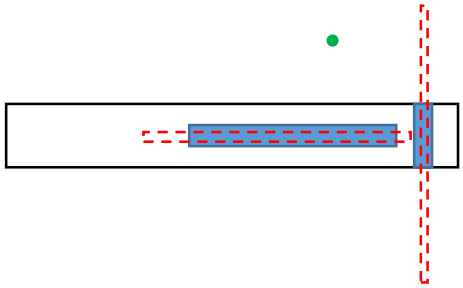

Figure 4. Scenario where active point is outside of the imaging planes

In this work, we present 2 main methods for localizing the active acoustic point source based on the data received by the bi-plane transrectal transducer. The main distinction between these two methods is that one uses requires pre-beamformed channel data, while the other uses beamformed data directly. The focus of our work is on the method using beamformed data, but the general method using pre-beamformed channel data is also presented for completeness.

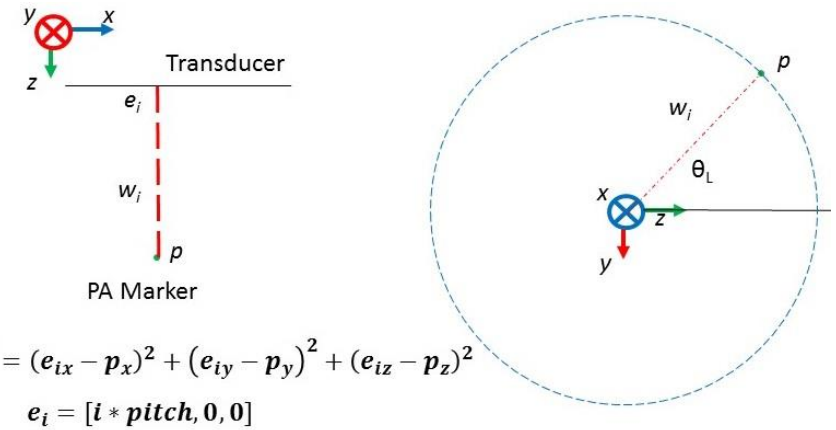

$$w_i^2 = (e_{ix} - p_x)^2 + \left(e_{iy} - p_y\right)^2 + (e_{iz} - p_z)^2$$

$$e_i = [i * pitch, 0, 0]$$

$$w_i^2 = (e_{ix} - p_x)^2 + p_y^2 + p_z^2$$

Figure 5. Geometrical model of an active point source observed by a linear ultrasound transducer

We will first describe the geometrical model of an active point source. The situation when the ultrasound transducer is linear is shown in figure 5. The PA spot or any active point source is denoted as *p* and transducer element *i* is denoted as e_i. w_i represents the distance from the PA spot to transducer element *i*. Since we are looking at active points, its position in the beamformed image must be interpreted in a different manner than a typical pulse-echo ultrasound image. While we can still trust the lateral position of the point in the image, the axial position now contains an elevational component as well. From the beamformed image, we know the distance, *w*, from the PA spot to the closest element on the transducer, e_i. With just this information, there is one unknown degree of freedom, θ_L, representing a circle about element e_i that the PA spot can lie on. A similar model can be shown for a curvilinear ultrasound transducer, with the main difference being that e_i having some axial component, when using beamformed images only.

As this active point source is observed by both the linear and curvilinear array, there will be two such circles, each with one unknown degree of freedom. Ideally, the active point will lie on the intersection of these circles. Since the circles may not actually intersect, due to small calibration errors, we can solve this system in a least-squares sense to find the point coordinates. An alternative method (used in the experimental results below) computes the intersection of the circular arc determined from the curvilinear transducer with the plane containing the circular arc determined from the linear transducer image. In either case, solving the system also requires that we know the transformation between to two transducer coordinate systems, which can either be determined by calibration or obtained from the bi-plane transrectal transducer specifications.

There also exists a more general method for solving for the position of the active point source. This method uses the acquired channel data before beamforming is applied. Referring back to figure 3, each channel will have a signal received from the active point source corresponding to its time of flight (TOF). This same scenario can be seen in figure 4. Previously, we only used the w_i corresponding to the shortest TOF, but now we use the entire array of *w*. Given this information, one can set up an optimization problem of the form shown in equation 1. In this equation, e_i represents the position of each of the transducer elements, *p* represents the position of the active point source, and *w* represents the distance between each e_i and *p*. This type of method is only suitable for transducers with non-collinear elements like bi-plane transrectal transducers or curvilinear transducer, but not for linear transducers.

$$\vec{p} = \underset{\vec{p}}{\operatorname{argmin}} \left(\left|\left|\vec{e}_i - \vec{p}\right|\right|_2 - w_i \right)^2 \quad (1)$$

3. Experiments and Results

3.1 Experimental Setup and Apparatus

We designed two experiments to test the feasibility of the proposed method. The first experiment focuses on the active point localization algorithm. To isolate this method from other effects such as stereo camera tracking errors, we introduce the use of an active piezoelectric (PZT) element as a replacement for the PA marker. While the active signal generation of a PZT element is similar to a PA marker, we must use another way to track the PZT element as we want to avoid using a stereo camera. In this case, we chose to use a translational stage that placed the PZT element sequentially in a grid-like pattern. The known positions in this grid becomes a replacement for the PA markers tracked by the stereo camera. This registration provides the pose of the ultrasound transducer relative to the grid-like pattern, and not relative to some external tracking frame. The ultrasound channel data is collected using a SonixTouch ultrasound system, SonixDAQ data acquisition system, and BPC8-4/10 and BPL9-5/55 bi-plane transrectal transducer.

The second experiment incorporates photoacoustic markers and a stereo camera system, accomplishing the originally stated goal of tracking the ultrasound transducer. In this experiment, PA markers are generated sequentially, with stereo camera images and ultrasound channel data being acquired simultaneously. The photoacoustic setup consists of a Q-switched Nd:YAG laser and corresponding optical mirrors and lenses. The stereo camera system consists of two calibrated CMLN-13S2C cameras. Points from the 10Hz Nd:YAG laser are sequentially projected onto a black plastisol phantom and collected using the same ultrasound transducer and SonixDAQ as the first experiment. The energy from these spots are well below the IEC laser safety limits [21]. The software used to synchronize and acquire data from each of these data sources is based on the MUSiiC Toolkit [22].

3.2 Results

The first experiment (with an active PZT element) had a total of 16 points, resulting in target registration errors of 1.07mm±0.35mm with a leave one out analysis. The equation for this metric is found in equation 2. F is the computed transformation of the ultrasound transducer in the stereo camera's coordinate system, while SC and US are the left out photoacoustic marker in the stereo camera and ultrasound coordinate systems respectively. TRE is the mean of each test point (active PZT source or PA marker) being used as the test point iteratively. Naturally, the first experiment did not use the stereo camera and all of the active PZT points are defined with respect to its grid-like pattern. The second experiment (with PA markers) had a total of 7 points, resulting in target registration errors of 1.27mm±0.47mm with a leave one out analysis. Figure 6 is a graphical representation of the registration result of the first experiment.

$$\overrightarrow{TRE} = \mathbf{F}_{SC\_US} * \overrightarrow{SC}_{test} - \overrightarrow{US}_{test} \quad (2)$$

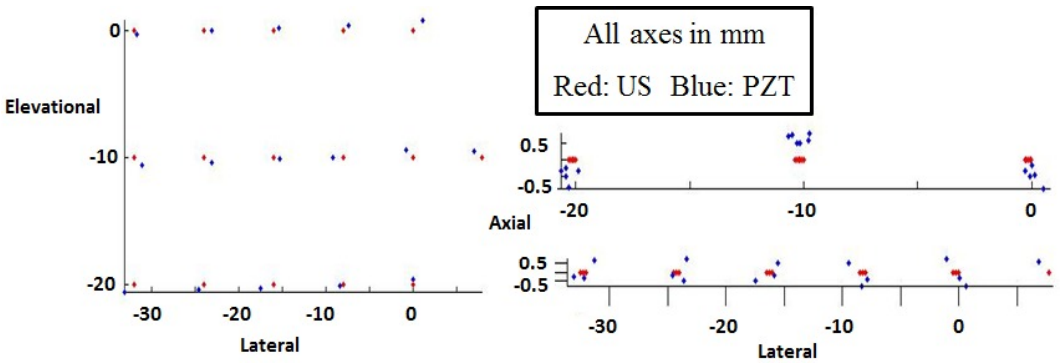

Figure 6. Result of point set registration for the first experiment

4. Discussion

From these two experiments, we can see that the active point localization algorithm and video to bi-plane transrectal ultrasound registration using photoacoustic markers is feasible. The first experiment shows that the localization method is accurate to approximately 1mm, which is significant, given that the PZT element itself is approximately 2mm in diameter. From figure 6, we can also see that there seems to be some bias in the localization method. One possible reason for this is that the model is based on ideal point sources and point receivers. Relaxing this assumption will naturally affect the model, but will also more closely resemble the physical apparatus.

From the second experiment, we can see that the errors increase when including the stereo camera and photoacoustic systems. There are two main possibilities for this result. First, stereo camera calibration errors are typically sub-millimeter. This is negligible in most applications, but fairly significant in this case as our errors are already fairly low. The second possibility is that the active point is much larger in the photoacoustic case. The laser spots were roughly 6mm while the active PZT element was 2mm. This can lead to error in both stereo camera segmentation and active point localization as the point source is now much larger. A more general explanation for part of the error is a certain assumption that we have to make regarding the speed of sound in the medium. In our model, we assume a homogeneous medium with a known speed of sound. It is difficult in practice to accurately pick a speed of sound for a certain medium. This is another possible cause for errors.

There are still several necessary advances to enable this technology in a practical setting. First of all, the sequential firing and generation of PA spots will take much too long in its current setup for real-time tracking. One obvious solution to this is to use a laser with a higher pulse repetition rate. Another solution is to use concurrent PA markers as we have previously shown [14]. One reason why this was not the first choice is because the bi-plane transrectal probe cannot really be regarded as a single transducer. It acts more similarly to two transducers that are active at the same time. As such, if multiple signals are seen by each of the transducers, then there will be ambiguity in how we find correspondence between a single PA marker seen in each transducer. A model-based approach similar to the one we previously developed [14] may work, but that remains to be tested in the future.

5. Conclusion

In this work, we showed the feasibility of registering video and ultrasound using a bi-plane transrectal transducer with photoacoustic markers. This approach obtained results better than conventional surgical navigation systems. Future work will include concurrent photoacoustic marker projection and *ex vivo* experiments.

Acknowledgements

Financial support was provided by Johns Hopkins University internal funds, NIBIB-NIH grant EB015638, and NSF grant IIS-1162095.

References

[1] Y. Wang, S. Butner, and A. Darzi, "The developing market for medical robotics," Proc. IEEE 94(9), 1763-1771 (2006).
[2] R. Taylor et al., Computer Integrated Surgery, MIT Press, Cambridge, Massachusetts (1996).
[3] P. J. Stolka et al., "A 3D-elastography-guided system for laparoscopic partial nephrectomies," Proc. SPIE 7625, 76251I (2010).

[4] C. L. Cheung et al., "Fused video and ultrasound images for minimally invasive partial nephrectomy: a phantom study," Med. Image. Comput. Comput. Assist. Interv. 13(3), 408-415 (2010).
[5] N. Navab, M. Mitschke, and O. Schutz, "Camera-augmented mobile C-arm (CAMC) application: 3D reconstruction using low cost mobile C-arm," Med. Image. Comput. Comput. Assist. Interv. 1679, 688-697 (1999).
[6] A. Wiles, D. Thompson, and D. Frantz, "Accuracy assessment and interpretation for optical tracking systems," Proc. SPIE 5367, 421-432 (2004).
[7] E. Boctor et al., "A novel closed form solution for ultrasound calibration," in Int. Symp. Biomed. Image., pp. 527-530, IEEE, Arlington, (2004).
[8] T. Poon and R. Rohling, "Comparison of calibration methods for spatial tracking of a 3-D ultrasound prove," Ultrasound Med. Biol. 31(8), 1095-1108 (2005).
[9] J. Leven et al., "DaVinci canvas: a telerobotic surgical system with integrated, robot-assisted, laparoscopic ultrasound capability," Med. Image. Comput. Comput. Assist. Interv. 8(1), 811-818 (2005).
[10] M. C. Yip et al., "3D ultrasound to stereoscopic camera registration through an air-tissue boundary," Med. Image. Comput. Comput. Assist. Interv. 13(2), 626-634 (2010).
[11] S. Vyas et al., "Interoperative ultrasound to stereo camera registration using interventional photoacoustic imaging," Proc. SPIE 8316, 83160S (2012).
[12] A. Cheng et al., Direct 3D ultrasound to video registration using photoacoustic effect, Med. Image. Comput. Comput. Assist. Interv. 2, 552559 (2012).
[13] A. Cheng et al., Direct 3D ultrasound to video registration using photoacoustic markers, J. Biomed. Opt. 18(6), 066013 (2013).
[14] A. Cheng et al., Concurrent Photoacoustic Markers for Direct three-dimensional Ultrasound to Video Registration, Proc. SPIE BiOS, 89435J-89435J-9 (2014).
[15] R. Kolkman, W. Steenbergen, and T. van Leeuwen, "In vivo photoacoustic imaging of blood vessels with a pulsed laser diode," Laser. Med. Sci. 21(3), 134-139 (2006).
[16] N. Kuo et al., "Photoacoustic imaging of prostate brachtherapy seeds in ex vivo prostate," Proc. SPIE 7964, 796409 (2011).
[17] M. Xu and L. Wang, "Photoacoustic imaging in biomedicine," Rev. Sci. Instrum. 77, 041101 (2006).
[18] C. Hoelen et al., "Three-dimensional photoacoustic imaging of blood vessels in tissue," Opt. Lett. 23(8), 648-650 (1998).
[19] A. Cheng et al., Direct ultrasound to video registration using photoacoustic markers from a single image pose, Proc. SPIE BiOS, 93130X (2015)
[20] A. Myronenko and X. Song, Point-set registration: coherent point drift, IEEE Trans. Pattern Anal. Mach. Intell., 32(12), 22622275 (2010).
[21] IEC60825-1:1993+A1:1997+A2:2001:Safety of Laser Products-Part 1: Equipment Classification and Requirements, International Electrotechnical Commission, Geneva, 2001, "IEC safety standard for lasers," http://lpno.tnw.utwente.nl/safety/iec60825-1%7Bed1.2%7Den.pdf (4 June 2013).
[22] H. J. Kang et al., Software framework of a real-time pre-beamformed RF data acquisition of an ultrasound research scanner, Proc. SPIE 8320, 83201F (2012).